Applied Physics
Express

LETTER • OPEN ACCESS

Evaluation of stress in (111) homoepitaxial CVD diamond films by Raman spectrum and nitrogen-vacancy centers

To cite this article: T. Tsuji *et al* 2024 *Appl. Phys. Express* **17** 115502

OPEN ACCESS

Applied Physics Express 17, 115502 (2024) LETTER

https://doi.org/10.35848/1882-0786/ad88d4

Evaluation of stress in (111) homoepitaxial CVD diamond films by Raman spectrum and nitrogen-vacancy centers

T. Tsuji[1], C. Shinei[2], T. Iwasaki[3], M. Hatano[3], and T. Teraji[2*]

[1]International Center for Young Scientists, National Institute for Materials Science, 1-1 Namiki, Tsukuba, Ibaraki 305-0044, Japan
[2]Research Center for Electronic and Optical Materials, National Institute for Materials Science, 1-1 Namiki, Tsukuba, Ibaraki 305-0044, Japan
[3]Department of Electrical and Electronic Engineering, School of Engineering, Tokyo Institute of Technology, 2-12-1 Ookayama, Meguro, Tokyo 152-8552, Japan

*E-mail: TERAJI.Tokuyuki@nims.go.jp

Received September 6, 2024; revised September 28, 2024; accepted October 18, 2024; published online December 5, 2024

The reduction of inhomogeneous stress in diamonds is crucially important for extracting excellent performance of semiconducting diamonds. In this study, to investigate elastic deformation in nitrogen doped (111) diamond films caused by stress, we evaluated the stress in these films using confocal Raman microscopy. The stress was detectable when the misorientation angle (θ_{mis}) was below 3.7° and it decreased as θ_{mis} increased. The Raman spectroscopic measurements, considered together with reported stress measurements by nitrogen-vacancy centers, suggest that the diamond film at low θ_{mis} was subjected to compressive stresses that were stronger in the [111] direction than [1$\bar{1}$0] or [$\bar{1}\bar{1}$2] directions.

Supplementary material for this article is available online

Nitrogen-vacancy (NV) centers in diamonds have functioned as quantum sensors that are sensitive to magnetic[1,2] and electric fields,[3,4] temperature,[5,6] and pressure,[7,8] with spatial resolutions from nanoscale[9,10] to millimeter scale.[11–13] Specifically, magnetic sensors with large excitation volume, being larger than $(0.1\,\mathrm{mm})^3$, are expected to achieve high sensitivity required for biomagnetic measurements[14–18] and battery current monitoring.[19]

The magnetic sensitivity of the NV center can be enhanced by increasing the spin dephasing time (T_2^*) of the ensemble NV center.[15] The T_2^* is limited mainly by the electron spin bath, including factors such as substitutional nitrogen defects [N_s^0] (P1 centers) and the NV center,[20] the nuclear spin bath of ^{13}C, and the inhomogeneous stress applied to the NV center in the diamond.[15] The stress applied to the NV center shifts the resonance frequency of a single NV center because of the spin–stress interaction with a shift magnitude proportional to the magnitude of the stress.[21–23] The spatially inhomogeneous stress causes broadening of the electron spin resonance signal of the ensemble NV centers, leading to reduction of T_2^*.[15]

We reported that T_2^* increases concomitantly with the increasing misorientation angle (θ_{mis}) of the High-Pressure High-Temperature (HPHT) (111) diamond substrate used for CVD diamond film growth. In this previous study, the diamond substrate surface was tilted from its (111) orientation into the [$\bar{1}\bar{1}$2] direction as presented in Fig. 1(a). Also, θ_{mis} is defined as the angle between [111] and that is normal to the polished diamond surface. Then, we demonstrated that this T_2^* improvement originated from reduction of the inhomogeneous stress applied to the NV center in the CVD diamond film.[24]

In this study, to investigate the elastic deformation caused by stress in these nitrogen-doped CVD (111) diamond films, we used confocal Raman spectroscopy to evaluate the stress applied to the diamond lattice. After a comprehensive analyses of the stress applied to both the diamond lattice and the NV centers in the CVD diamond films, we discuss the elastic deformation caused by stress in the CVD diamond film with low θ_{mis}.

Homoepitaxial CVD diamonds were grown on type-Ib HPHT (111) diamond substrates with dimensions of $1 \times 1 \times 0.3\,\mathrm{mm}^3$. The entire sample surface was thoroughly polished for both the front and back sides of the (111) diamond substrate in the **[$\bar{1}\bar{1}$2]** direction with $\boldsymbol{\theta}_{mis}$ of 2.0, 3.7, 5.0, and 10° as presented in Fig. 1(a). We created perfectly aligned NV centers in the CVD diamond films by using the substrates with θ_{mis}, which is effective in improving the sensitivity of the quantum sensors.[24,25] The fluorescence intensity of the NV center was measured using a confocal microscope. The CVD film thicknesses were estimated as approximately 60–70 μm from the fluorescence depth profile. The details of the growth conditions are described elsewhere.[24]

To analyze the stress applied to the diamond lattice in the CVD films, we used confocal Raman imaging (WITec alpha 300 R; Oxford Instruments Plc.). The wavelength and the excitation power of the laser being polarized into [$\bar{1}\bar{1}$2] direction were, respectively, 532 nm and 25 mW. The magnification and the numerical aperture of the objective lens were, respectively, 50 and 0.75. Figure 1(b) portrays an illustration of the diamond sample and the definitions of the x, y, and z axes. The Raman spectra were measured at 80×80 positions within the film plane (x–y plane) of $40 \times 40\,\mu\mathrm{m}^2$ at a given z, as presented in Fig. 1(c). (In the supplementary material, we show the area where the Raman measurements were performed with birefringence images of each CVD diamond films.) Fig. 1(d) shows the Raman spectra in the CVD films with θ_{mis} of 2.0 and 10°. The first-order Raman line of the diamond ($\approx$1332.5 cm^{-1}) and the fluorescence from the NV^0 center ($\approx$1400–1420 cm^{-1}) were observed. The first-order Raman line of the diamond was fitted with a Lorentzian function. The respective fitting errors of the peak position (P_{peak}) of the Lorentzian function for θ_{mis} of 2.0, 3.7, 5.0, and 10° were approximately 0.020, 0.020, 0.020, and 0.025 cm^{-1}. The differences of these fitting errors were due to the difference of the fluorescence intensity of the NV^0 center depending on θ_{mis}. The values of [N_s^0]

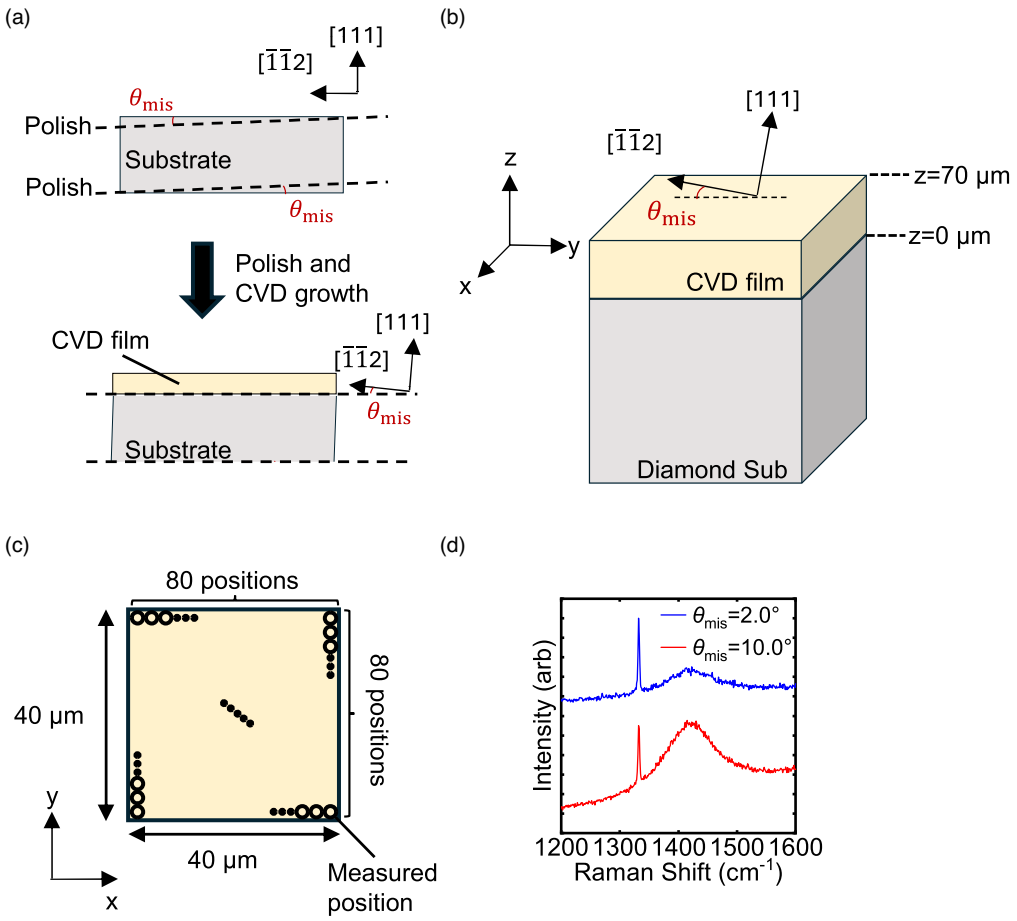

Fig. 1. (a) Schematic image of the CVD diamond film and (111) diamond substrate. (b) Illustration of the diamond sample and definition of the x–y–z axis. (c) Schematic image of the x–y plane where the Raman spectra were measured at 80 × 80 points for a 40 × 40 μm^2 at a given z. The open circle represents the measurements position. Instead of drawing 80 white circles, many measurement positions were represented by black circles. (d) Typical Raman spectrum in the CVD films with θ_{mis} of 2.0 and 10°.

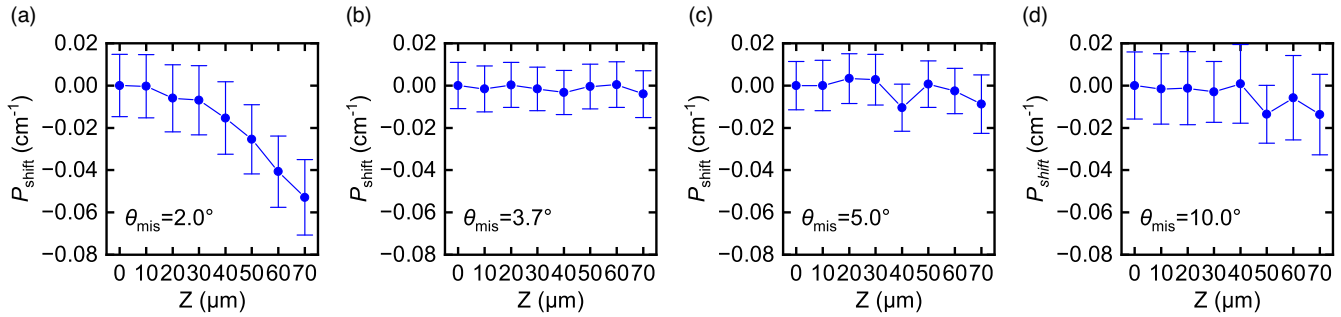

Fig. 2. The shift of diamond Raman peak (P_{shift}) with respect to the interface between the substrate and CVD diamond film (z = 0) as a function of the depth direction (z) for the CVD diamond with θ_{mis} of 2.0, 3.7, 5.0, and 10°, respectively. The plots and error bars, respectively, present the average value and the standard deviation of the diamond Raman peak positions for the 80 × 80 points at a given z.

estimated from the spin coherence time T_2 for θ_{mis} of 2.0, 3.7, 5.0, and 10° were, respectively, 31.6 ± 0.2, 22.4 ± 0.1, 22.9 ± 0.1, and 25.1 ± 0.2 ppm.[24)]

Figures 2(a)–2(d), respectively, show the shift of the diamond Raman peak (P_{shift}) with respect to the interface between the substrate and the CVD diamond film (z = 0) as a function of the depth direction (z) for the CVD diamond with θ_{mis} of 2.0, 3.7, 5.0, and 10°. Here, the plots and error bars, respectively, represent the average value and the standard deviation of the diamond Raman peak positions for the 80 × 80 points at a given z. As presented in Fig. 2(a), P_{shift} was decreased by approximately −0.056 cm^{-1} from the substrate to the CVD film surface at θ_{mis} of 2.0°. By contrast, the change of the P_{shift} was as small as within approximately ±0.020 cm^{-1} at θ_{mis} of 3.7°, 5.0, and 10°, as shown in Figs. 2(b)–2(d). These results indicate that the stress applied to diamond lattice for θ_{mis} of 2.0° was higher than that for higher θ_{mis}. Considering the fitting error of P_{peak} (0.020–0.025 cm^{-1}) as described above, the stresses applied to the diamond lattice in CVD films at θ_{mis} of 3.7, 5.0, and 10° were smaller than the detection limit of these measurements.

Next, we discuss the elastic deformation of the CVD diamond film with a θ_{mis} of 2.0° based on the measurement

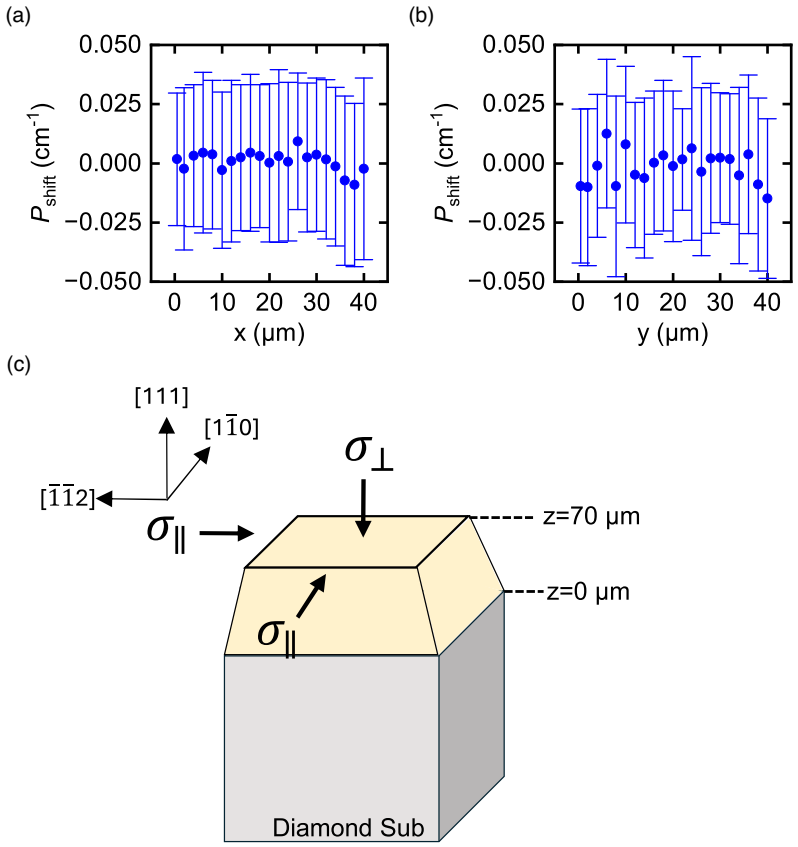

Fig. 3. (a) and (b) The shift of the diamond Raman peak (P_{shift}) as a function of the x and y direction, respectively, at the CVD diamond surface (z = 70) of the sample with a θ_{mis} of 2.0°. The plots and error bars, respectively, represent the average value and the standard deviation of the diamond Raman peak positions.Raman measurements were performed with 80 points along both the x and y direction. However, for clarity in the figure, only data for 21 points along each of the x and y direction was shown.. (c) Assumption of the stress in the CVD diamond film in this study. We assume that the stress was applied parallel $\sigma_\parallel$ (the [1$\bar{1}$0] and [$\bar{1}\bar{1}$2] direction) and perpendicular $\sigma_\perp$ ([111] direction) to the (111) CVD surface at z = 70.

results of the stress applied to the diamond lattice and the NV centers. The stress applied to the diamond lattice was estimated from the P_{shift} of the Raman measurements performed for this study, whereas the stress applied to the NV centers was evaluated from the shift of the spin–stress interaction $\boldsymbol{M}_z$ reported from our earlier work.[24] As might be apparent from Eq. (3) shown below, the value of $\boldsymbol{M}_z$ varies with the amount of stress applied to the NV centers. As presented in Fig. 2(a), the distribution of averaged values of the P_{shift} in the depth direction (z) was larger than the standard deviation of P_{shift} at a given z (in the x–y plane). This result indicates that the stress was more distributed in the direction of the CVD film growth, i.e., the [111] direction than in the [1$\bar{1}$0] or [$\bar{1}\bar{1}$2] direction. Therefore, we evaluate the magnitude of the stress in the CVD film surface (z = 70) with respect to the interface between the substrate and the CVD film (z = 0) as the reference point. Figures 3(a) and 3(b) respectively show the shift of the diamond Raman peak (P_{shift}) in the x and y directions at the CVD diamond surface (z = 70) of the sample with θ_{mis} of 2.0°. Here, the plots and error bars, respectively, represent the average value and the standard deviation of the diamond Raman peak positions for the 80 points at a given x or y. The change of the average value of P_{shift} were as small as within the standard deviation of P_{shift} depending on the x and y direction. This result suggests that the magnitudes of the stress in the [1$\bar{1}$0] and [$\bar{1}\bar{1}$2] directions were almost equal. Therefore, we assume that the stress was applied parallel (the [1$\bar{1}$0] and [$\bar{1}\bar{1}$2] direction) and perpendicular ([111] direction) to the (111) CVD surface at z = 70, represented respectively as ($\sigma_\parallel$) and ($\sigma_\perp$), as depicted in Fig. 3(c). In this case, a stress tensor at the CVD surface (T) can be expressed in the following form.

$$\mathrm{T} = \begin{pmatrix} \sigma_\parallel & 0 & 0 \\ 0 & \sigma_\parallel & 0 \\ 0 & 0 & \sigma_\perp \end{pmatrix} \tag{1}$$

It is given with respect to the diamond unit cell coordinate system (X = [1$\bar{1}$0], Y = [$\bar{1}\bar{1}$2], Z = [111]) and such that the compressive stress is positive. The shift of the first-order Raman line P_{shift} is expressed by the following equation using $\sigma_\parallel$ and $\sigma_\perp$

$$\frac{[2(p+2q)(s_{11}+2s_{12})+2rs_{44}]\sigma_\parallel + [(p+2q)(s_{11}+2s_{12})-2rs_{44}]\sigma_\perp}{6\omega_0} = P_{shift} \tag{2}$$

where p, q, and r are the deformation potential constants ($p/\omega_o^2 = -2.80$, $q/\omega_o^2 = -1.770$ and $r/\omega_o^2 = -1.900$), s_{11}=

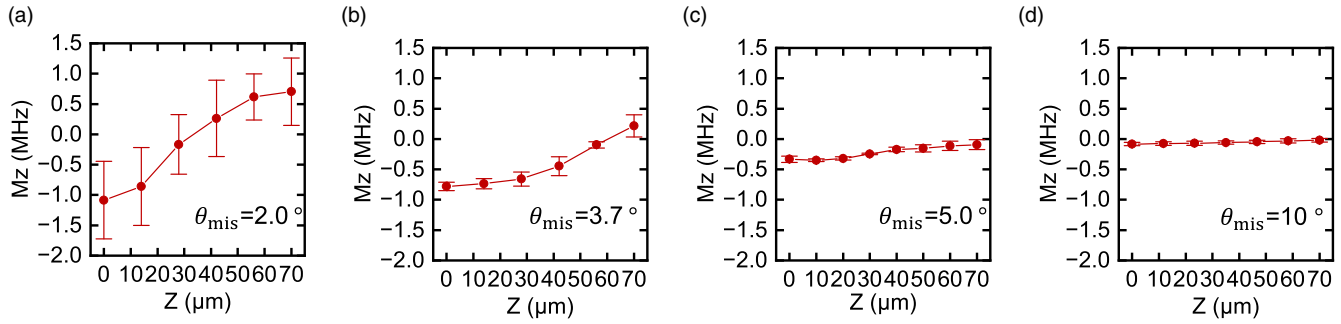

Fig. 4. The shifts of the spin–stress interaction M_z in the z-direction for the CVD diamond with θ_{mis} of 2.0, 3.7, 5.0, and 10°. The plots and error bars, respectively, present the average value and the standard deviation of M_z at a given z. This data was reproduced from Fig. 3(c) of our earlier report.[24)]

-0.952, $s_{12} = 0.099$, $s_{44} = -1.737$ are compliance constants (10^{-3} GPa^{-1}), and $\omega_0 = 1332.5$ is the frequency of the triply degenerated phonon (cm^{-1}).[26)] The supplementary material provides details of the derivation of this formula. It is known that when these two stresses ($\sigma_{\parallel}$ and $\sigma_{\perp}$) are applied to the diamond lattice, the Raman peak of the diamond, i.e., the frequency of the triply degenerated phonon, is generally split into two peaks by the change of the TO and LO phonon modes.[27)] For this experiment, the laser polarized in the $[\bar{1}\,\bar{1}\,2]$ direction was used for Raman measurements. In this configuration, the TO phonon mode produced four times higher fluorescence intensity than the LO phonon mode based on the Raman's selection rule. Therefore, we considered that the diamond Raman peak detected in this study was mainly attributable to the TO phonon mode (the supplementary material provides additional details.). As presented in Fig. 2(a), the diamond Raman peak of the samples with θ_{mis} of 2.0° decreased from the substrate to the CVD film surface by P_{shift} of -0.056 ± 0.02 (cm^{-1}).

The shift of the spin–stress interaction $\boldsymbol{M}_{z_{shift}}$ is expressed as following equation using $\sigma_{\parallel}$ and $\sigma_{\perp}$

$$(2a_1 - a_2)\sigma_{\parallel} + (a_1 + a_2)\sigma_{\perp} = \boldsymbol{M}_{z_{shift}} \quad (3)$$

where $a_1 = 4.86$ and $a_2 = -3.70$ are the stress susceptibility parameters (MHz/GPa).[21,22)] The supplementary material presents details of the derivation of this formula. Figures 4(a)–4(d), respectively, present variations of the spin–stress interaction $\boldsymbol{M}_z$ in the z-direction for the CVD diamond with θ_{mis} of 2.0, 3.7, 5.0, and 10°. The average value $\boldsymbol{M}_z$ was distributed from approximately -0.6 to $+1.1$ MHz in a sample with θ_{mis} of 2.0°. The distribution of $\boldsymbol{M}_z$ became narrower as θ_{mis} increased. This result indicates that, as in the case of the stress investigation using the Raman spectroscopy presented in Fig. 2, the stress applied to the NV centers decreased as θ_{mis} increased. The $\boldsymbol{M}_z$ of the CVD diamond film with θ_{mis} of 2.0° was increased from the substrate to the CVD film surface by $\boldsymbol{M}_{z_{shift}}$ of 1.7 ± 0.7 (MHz). By substituting the values of P_{shift} and $\boldsymbol{M}_{z_{shift}}$ into Eqs. (2) and (3), $\sigma_{\parallel}$ and $\sigma_{\perp}$ were estimated, respectively, as 0.064 ± 0.03 and 0.71 ± 0.4 GPa. The positive values of $\sigma_{\parallel}$ and $\sigma_{\perp}$ indicated that the CVD diamond film at low θ_{mis} was subjected to compressive stress, which was higher in the [111] direction than in either the $[1\,\bar{1}\,0]$ or $[\bar{1}\,\bar{1}\,2]$ direction at the CVD diamond film surface. In addition, the fact that the diamond was subjected to the compressive stress indicated that the lattice constant of the CVD diamond surface was smaller than that of the HPHT substrate. This finding is consistent with a report describing the lattice constant of nitrogen-doped CVD diamond films as smaller than that of Ib HPHT (111) diamond substrates.[28)]

In conclusion, we evaluated the stress applied to a diamond lattice in the nitrogen-doped CVD film grown on an Ib HPHT (111) substrate using confocal Raman microscopy. The diamond Raman peak was shifted by approximately -0.053 cm^{-1} from the substrate to the CVD film surface when θ_{mis} was 2.0°. However, the shift was within approximately ± 0.020 cm^{-1} at θ_{mis} of 3.7°, 5.0, and 10°. Therefore, the stress applied to the diamond lattice was reduced at $\theta_{mis} \geq 3.7°$. For the diamond CVD film at θ_{mis} of 2.0°, the P_{shift} shifted by -0.053 cm^{-1}; also, the spin–stress interaction $\boldsymbol{M}_z$ shifted by 1.7 MHz in the diamond growth direction of [111]. From these values, we estimated the stress parallel ($[1\,\bar{1}\,0]$ and $[\bar{1}\,\bar{1}\,2]$ direction) and the perpendicular ([111] direction) to the (111) CVD surface as 0.064 ± 0.03 and 0.71 ± 0.4 GPa, respectively. We believe that such compressive stress at low θ_{mis} was reduced by increasing θ_{mis}.

Acknowledgments We gratefully acknowledge the constructive discussions and insightful comments provided by Dr Junichi Inoue, Dr Kimiyoshi Ichikawa and Dr Takeharu Sekiguchi. This work was partially supported by MEXT Q-LEAP (Grant Nos. JPMXS0118068379, JPMXS0118067395), JST Moonshot R&D (Grant No. JPMJMS2062), MIC R&D for construction of a global quantum cryptography network (Grant No. JPMI00316), CSTI SIP "Promoting the application of advanced quantum technology platforms to social issues," JSPS KAKENHI (Grant Nos. 20H05661, 24H00406).

ORCID iDs T. Tsuji https://orcid.org/0000-0002-7342-6198 T. Teraji https://orcid.org/0000-0002-7731-0547

1) F. Jelezko, T. Gaebel, I. Popa, M. Domhan, A. Gruber, and J. Wrachtrup, "Observation of coherent oscillation of a single nuclear spin and realization of a two-qubit conditional quantum gate," Phys. Rev. Lett. **93**, 130501 (2004).
2) D. Budker and M. Romalis, "Optical magnetometry," Nat. Phys. **3**, 227 (2007).
3) F. Dolde et al., "Electric-field sensing using single diamond spins," Nat. Phys. **7**, 459 (2011).
4) B. Yang et al., "Vector electrometry in a wide-gap-semiconductor device using a spin-ensemble quantum sensor," Phys. Rev. Appl. **14**, 044049 (2020).
5) M. W. Doherty, V. M. Acosta, A. Jarmola, M. S.-J. Barson, N. B. Manson, D. Budker, and L. C.-L. Hollenberg, "Temperature shifts of the resonances of theNV−center in diamond," Phys. Rev. B **90**, 041201(R) (2014).
6) Y. Hatano et al., "Simultaneous thermometry and magnetometry using a fiber-coupled quantum diamond sensor," Appl. Phys. Lett. **118**, 034001 (2021).
7) R. Kitagawa et al., "Pressure sensor using a hybrid structure of a magnetostrictive layer and nitrogen-vacancy centers in diamond," Phys. Rev. Appl. **19**, 044089 (2023).
8) S. Hsieh et al., "Imaging stress and magnetism at high pressures using a nanoscale quantum sensor," Science **366**, 1349 (2019).
9) J. M. Taylor, P. Cappellaro, L. Childress, L. Jiang, D. Budker, P. R. Hemmer, A. Yacoby, R. Walsworth, and M. D. Lukin, "High-sensitivity diamond magnetometer with nanoscale resolution," Nat. Phys. **4**, 810 (2008).

10) I. Lovchinsky et al., "Nuclear magnetic resonance detection and spectroscopy of single proteins using quantum logic," Science **351**, 836 (2016).
11) T. Wolf, P. Neumann, K. Nakamura, H. Sumiya, T. Ohshima, J. Isoya, and J. Wrachtrup, "Subpicotesla diamond magnetometry," Phys. Rev. **5**, 1 (2015).
12) C. Zhang et al., "Diamond magnetometry and gradiometry towards subpicotesla dc field measurement," Phys. Rev. Appl. **15**, 064075 (2021).
13) I. Fescenko, A. Jarmola, I. Savukov, P. Kehayias, J. Smits, J. Damron, N. Ristoff, N. Mosavian, and V. M. Acosta, "Diamond magnetometer enhanced by ferrite flux concentrators," Phys Rev Res **2**, 023394 (2020).
14) K. Arai et al., "Millimetre-scale magnetocardiography of living rats with thoracotomy," Commun. Phys. **5**, 1 (2022).
15) J. F. Barry, J. M. Schloss, E. Bauch, M. J. Turner, C. A. Hart, L. M. Pham, and R. L. Walsworth, "Sensitivity optimization for NV-diamond magnetometry," Rev. Mod. Phys. **92** (2020).
16) J. L. Webb et al., "Optimization of a Diamond nitrogen vacancy centre magnetometer for sensing of biological signals," Front. Phys. **8**, 522536 (2020).
17) J. L. Webb et al., "Detection of biological signals from a live mammalian muscle using an early stage diamond quantum sensor," Sci. Rep. **11**, 2412 (2021).
18) N. Sekiguchi et al., "Diamond quantum magnetometer with dc sensitivity of sub-10 pT Hz0.2em0ex˜1/2 toward measurement of biomagnetic field," Phys. Rev. Appl. **21**, 064010 (2024).
19) Y. Hatano et al., "High-precision robust monitoring of charge/discharge current over a wide dynamic range for electric vehicle batteries using diamond quantum sensors," Sci. Rep. **12**, 13991 (2022).
20) C. Shinei, Y. Masuyama, M. Miyakawa, H. Abe, S. Ishii, S. Saiki, S. Onoda, T. Taniguchi, T. Ohshima, and T. Teraji, "Nitrogen related paramagnetic defects: decoherence source of ensemble of NV− center," J. Appl. Phys. **132**, 214402 (2022).
21) M. S.-J. Barson et al., "Nanomechanical sensing using spins in diamond," Nano Lett. **17**, 1496 (2017).
22) D. A. Broadway et al., "Microscopic imaging of the stress tensor in diamond using in situ quantum sensors," Nano Lett. **19**, 4543 (2019).
23) M. W. Doherty, F. Dolde, H. Fedder, F. Jelezko, J. Wrachtrup, N. B. Manson, and L. C.-L. Hollenberg, "Theory of the ground-state spin of the NV−center in diamond," Phys. Rev. B **85**, 205203 (2012).
24) T. Tsuji, T. Sekiguchi, T. Iwasaki, and M. Hatano, "Extending spin dephasing time of perfectly aligned nitrogen-vacancy centers by mitigating stress distribution on highly misoriented chemical-vapor-deposition diamond," Adv. Quantum Technol. (2023).
25) T. Miyazaki, Y. Miyamoto, T. Makino, H. Kato, S. Yamasaki, T. Fukui, Y. Doi, N. Tokuda, M. Hatano, and N. Mizuochi, "Atomistic mechanism of perfect alignment of nitrogen-vacancy centers in diamond," Appl. Phys. Lett. **105**, 261601 (2014).
26) M. Mermoux, B. Marcus, A. Crisci, A. Tajani, E. Gheeraert, and E. Bustarret, "Micro-Raman scattering from undoped and phosphorous-doped (111) homoepitaxial diamond films: stress imaging of cracks," J. Appl. Phys. **97**, 043530 (2005).
27) M. H. Grimsditch, E. Anastassakis, and M. Cardona, "Effect of uniaxial stress on the zone-center optical phonon of diamond," Phys. Rev. B: Condens. Matter **18**, 901 (1978).
28) S. Shikata, T. Tanno, T. Teraji, H. Kanda, T. Yamada, and J.-I. Kushibiki, "Precise measurements of diamond lattice constant using bond method," Jpn. J. Appl. Phys. **57**, 111301 (2018).